HHS Public Access

Author manuscript

Conf Proc IEEE Eng Med Biol Soc. Author manuscript; available in PMC 2018 November 19.

Published in final edited form as:

Conf Proc IEEE Eng Med Biol Soc. 2018 July ; 2018: 427–4631. doi:10.1109/EMBC.2018.8513129.

Isometry Invariant Shape Descriptors for Abnormality Detection on Brain Surfaces Affected by Alzheimer's Disease

Yanshuai Tu[1], **Chengfeng Wen**[2], **Wen Zhang**[1], **Jianfeng Wu**[1], **Jie Zhang**[1], **Kewei Chen**[3], **Richard J. Caselli**[4], **Eric M. Reiman**[3], **Xianfeng David Gu**[2], and **Yalin Wang**[1]

[1]CIDSE, Arizona State University, Tempe, AZ

[2]Department of Computer Science, Stony Brook Univ., Stony Brook, NY

[3]Banner Alzheimers Institute, Phoenix, AZ

[4]Mayo Clinic, Scottsdale, AZ

Abstract

Alzheimer's disease (AD), a progressive brain disorder, is the most common neurodegenerative disease in older adults. There is a need for brain structural magnetic resonance imaging (MRI) biomarkers to help assess AD progression and intervention effects. Prior research showed that surface based brain imaging features hold great promise as efficient AD biomarkers. However, the complex geometry of cortical surfaces poses a major challenge to defining such a feature that is sensitive in qualification, robust in analysis, and intuitive in visualization. Here we propose a novel isometry invariant shape descriptor for brain morphometry analysis. First, we calculate a global area-preserving mapping from cortical surface to the unit sphere. Based on the mapping, the Beltrami coefficient shape descriptor is calculated. An analysis of average shape descriptors reveals that our detected features are consistent with some previous AD studies where medial temporal lobe volume was identified as an important AD imaging biomarker. We further apply a novel patch-based spherical sparse coding scheme for feature dimension reduction. Later, a support vector machine (SVM) classifier is applied to discriminate 135 amyloid-beta positive persons with the clinical diagnosis of Mild Cognitive Impairment (MCI) from 248 amyloid-beta-negative normal control subjects. The 5-folder cross-validation accuracy is about 81.82% on the dataset, outperforming some traditional, Freesurfer based, brain surface features. The results show that our shape descriptor is effective in distinguishing dementia due to AD from age-matched normal aging individuals. Our isometry invariant shape descriptors may provide a unique and intuitive way to inspect cortical surface and its morphometry changes.

I. INTRODUCTION

Alzheimer's disease (AD), a highly prevalent and irreversible neurological degeneration, is a major health concern. According to an estimation from the Alzheimer's Association [1], 5.5 million Americans are currently living with Alzheimer's dementia and that number may reach more than 13 million by the year of 2050. Although the precise mechanism of AD development is not fully understood, AD progression is reflected in brain atrophy. It is hoped that treatment could have great benefit if started during the earliest stages of AD [2]. Because brain shape analysis techniques may identify subtle shape alterations, they may

have great potential for early detection of AD [3], as well as tracking AD progression [4], and the impact of therapeutic interventions [5]. With the development of magnetic resonance imaging (MRI), we can easily extract several brain shape features that measure AD's influence on brains structure, including the features of whole brain [6], temporal lobe volumes [7], hippocampus [8], cortical thickness [9].

Although various brain volume-based feature approaches [10], [11] were developed for brain volume image analysis, prior research [12], [13] has demonstrated that surface-based brain mapping may offer advantages over volume-based brain mapping work. Indeed, prominent surface-based analysis approaches, such as surface conformal mapping [14], isometry invariance analysis (e.g., surface spectral distances [15], and spherical harmonic analysis[16]), have been developed and demonstrated their greater success.

Among the surface approaches, isometry analysis studies, are of great interest as the results are invariant under isometric transformation of cortical surfaces. Unfortunately, due to the complicated geometry of cortical surfaces, currently available isometry analysis studies [17], [18] often fail to reach one of the desired requirements: sensitive in morphometry quantification, robust in abnormality detection, and intuitive in feature visualization.

Here we propose a novel shape descriptor, based on the area-preserving mapping [19] and Beltrami coefficients, to complement current isometric invariant methods. The area-preserving mapping, which preserves the local area of the surface, provides a globally optimal diffeomorphic mapping from cortical surface to the unit sphere. The mapping result is invariant under isometric transformation, i.e. rotate, scale, and transform. The Beltrami coefficients depict the anisotropicity of the elastic deformation of the mapping and can potentially be used as a shape signature to measure brain morphometry changes.

In our experiments, we apply our shape descriptors to 135 amyloid-positive AD (Aβ+) patients and 248 healthy control (Aβ−) subjects. The group difference results are consistent with some prior AD research [12]. We further apply a novel patch-based spherical sparse coding algorithm for feature dimension reduction. After that, a Support Vector Machine (SVM) classifier is used to classify these two groups. We see the 5-folder cross-validation accuracy rate for distinguishing AD and CTL subjects is about 81.82%, outperforming some traditional brain surface features. Our experimental results demonstrate that our shape descriptors may then be applied as potential imaging biomarkers for neurodegenerative disease research.

II. Method

A. Basic Ideas

Let S be a genus zero cortical surface, represented by the triangular mesh $M = (V,E,T)$. Our goal is to find a discrete map to the unit sphere $f: M \rightarrow \mathbb{S}^2/_{R=1}$, such that the area adjacent to each vertex $v_i \in V$ is conserved. It makes the problem tractable that f can be decomposed as three discrete mapping functions, conformal map to a planar domain c, area-preserving adjustment a on the planar domain, and the inverse stereo-graphic projection s^{-1} (see Fig. 1). Mathematical details for each of these mapping function appear in the next sections.

B. Conformal map to planar domain

We first find a $c : M \rightarrow \mathbb{C}$ which maps the brain surface M onto a planar domain. Such c can be found in two steps.

First, conformally map cortical surface to the unit sphere via *Spherical Harmonic Mapping*. We refer the reader to the paper [20] for a full description of this approach.

Second, punch a tiny hole around the north-pole of sphere and stereo-graphically project the unit sphere mapping to complex plane $\mathbb{C}$. Let point $v = (x, y, z)$ on the sphere and (u, v) on the complex plane, the stereographic projection is given by, $(u, v) = (\frac{x}{1-z}, \frac{y}{1-z})$. We denote D as the mapping result of c on input cortical surface M.

C. Area-Preserving Mapping

The area-preserving mapping, a further strategy of adjusting conformal result D, is based on *Brenier's Approach* to solving optimal mass transport (OMT) problem.

Suppose two metric spaces (X,μ) and (Y,ν) have a same total measure, $\int_X \mu = \int_Y \nu$. A transport plan $T : X \rightarrow Y$ is called a measure preserving transport plan if for any subset $U \subset Y$, $\mu(T^{-1}(U)) = \nu(U)$.

We are interested in finding a measure preserving transport plan T_{opt} such that the total transport cost is minimal, i.e. $T_{opt}(X,Y)=\text{argmin}_T \int_M c(x,T(x))d\mu(x)$, where $c(x, y)$ is the transportation cost of moving from $x \in X$ to $y \in Y$. Note the space Y can be discretized as $Y = \{y_1, y_2, \cdots, y_n\}$ with Dirac measure $\nu = \sum_{j=1}^{n} \nu_j \delta(y - y_j)$.

The following theorem, has been proven using a variational principle in [19], plays a fundamental role in finding the optimal discrete transport plan.

Theorem II.1—*Assume μ has a compact support $\Omega = \{x \in X | \mu(x) > 0\}$. For any given measure ν, with total measure preserved, i.e. $\sum_{j=1}^{n} \nu_j = \int_\Omega \mu$, $\nu_i > 0$, define a vector $\mathbf{h} = (h_1, h_2, \ldots, h_n) \in \mathbb{R}^n$, where h_i is a real number assigned to $y_i \in Y$. For each point y_i, constructs a hyperplane $< x, y_i > + h_i = 0$ in X, all these hyperplanes form a convex polyhedron $u(x)$. There must exist a height vector $\mathbf{h}$ unique up to adding a constant $(c, \ldots, c)$, such that the gradient map $\nabla u(x)$ optimizes the following transportation cost,*

$$E(T) := \int_\Omega |x - T(x)|^2 \mu(x) dx. \quad (1)$$

Meanwhile, the following measure-preservation constrains are satisfied for all cells, that is $\int_{W_i} \mu = \nu_i$, $i = 1, 2, \ldots, n$.

We explain the theorem in the context of our spherical area-preserving mapping. Our goal is to find $a : X \rightarrow Y$, such that once we do the inverse stereo-graphic mapping back to the unit sphere, the vertex area on the unit sphere, is same as vertex area on cortical surface M.

Let the mapping target of $x_i \in X$ be $y_i \in Y$. For each point y_i, a real value h_i is assigned (initially can be 0). With the assigned value h_i, we construct a hyperplane defined on X: $\pi_i : < x, y_i > + h_i = 0$, where $<,>$ is the inner product. Fig. 2 demonstrates the hyperplane π_i of point p_i on the compact support Ω. These hyperplanes intersect each other and eventually form a convex polyhedron $u(x)$, which have the condition, $u(x) = \max_i\{< x, y_i > + h_i\}$.

Denote $G(\mathbf{h})$ as the polyhedron graph of $u(x)$. Then the vertical projection of $G(\mathbf{h})$ induces a polygonal partition of Ω. We call ∇u, the gradient of u, a gradient map which maps each cell W_i to a single point y_i, i.e., $\nabla u(x) : W_i \rightarrow y_i$, $i = 1,2,\ldots,n$. One can see that the height vector $\mathbf{h}$ controls the hyperplanes, the shape of u, the induced cell decomposition W_i, and eventually the cell center.

It has been proven in [21] that the minimal solution of the following $E(\mathbf{h})$ also optimizes the cost defined in Equ. 1,

$$E(\mathbf{h}) = \int_{\Omega} u(x)\mu(x)dx - \sum_{i=1}^{n} \nu_i h_i . \quad (2)$$

If we find the $\mathbf{h}$ such that the energy is minimized, we are able to construct the area-preserving mapping according to the discussion. The benefits of taking the Eq. 2 is that the gradient and Hessian matrix can be given, respectively,

$$\nabla E(\mathbf{h}) = -\nu_i + \int_{W_i} \mu, \quad (3)$$

$$H_{ij} = \frac{\partial^2 E(\mathbf{h})}{\partial h_i \partial h_j} = \begin{cases} \int_{e_{ij}} \mu & W_i \cap W_j \cap \Omega \neq \varnothing \\ 0 & \text{otherwise} \end{cases} \quad (4)$$

Algorithm 1

Optimal Mass Transportation Map

Input: Planar convex domain with measure (Ω, μ);
Target points set with Dirac
measure$(\boldsymbol{p}, \boldsymbol{\nu}) = \{(p_1, \nu_1), (p_2, \nu_2), ..., (p_l, \nu_n)\}$;
A threshold ε, and a step α length.

Result: OMT map $\phi : (\Omega, \mu) \to (\boldsymbol{p}, \boldsymbol{\nu})$

begin
  $\boldsymbol{h} \leftarrow (0, 0, ..., 0)$.
  repeat
    Calculate $u(x)$;
    Compute ∇E according to Eqn. (3);
    Compute H according to Eqn. 4;
    Update height $\mathbf{h} \leftarrow \mathbf{h} - \alpha H^{-1} \nabla E(\mathbf{h})$
  until $|\nabla E(\boldsymbol{h})| < \varepsilon$;
  return $\phi : (\Omega, \mu) \to (\boldsymbol{p}, \boldsymbol{\nu})$,
   $W_i(\boldsymbol{h}) \to p_i, i = 1, 2, \cdots, k$
end

As the energy E is convex when the domain of Y is convex, the global minimum can be obtained efficiently by Newton's method. This procedure is described in Alg. 1. [21] In our setting, the vertex area of v_i, on surface S, is defined as,

$$A_i = \frac{1}{3} \sum_{j,k} Area([v_i, v_j, v_k]), \quad (5)$$

where $[v_i, v_j, v_k]$ is a triangle face adjacent to v_i. As our goal is the area-preserving respect to unit sphere, when we set the target measure on the planar domain, additional area distortion induced by stereo-graphic projection is taken into consideration, $\nu_i = \frac{4A_i}{(1 + u^2 + v^2)^2}$.

After solving the optimal mass transport problem on planar domain by Alg. 1, we do inverse stereo-graphic projection and yield the spherical area-preserving mapping of M. The inverse stereo-graphic projection is given by,

$$(x, y, z) = \left(\frac{2u}{1 + u^2 + v^2}, \frac{2v}{1 + u^2 + v^2}, \frac{-1 + u^2 + v^2}{1 + u^2 + v^2}\right). \quad (6)$$

D. Shape Descriptor

The area-preserving mapping carries precious information about the surface local area deformation. To quantify such deformation, we adopt the **Beltrami coefficient** [22] as our shape descriptor. Beltrami coefficient of surface, when given metric tensor $g(x, y) = \begin{pmatrix} E & F \\ F & G \end{pmatrix}$, can be defined as,

$$\mu(x, y) = \frac{E - G + 2iF}{E + G + 2\sqrt{EG - F^2}}. \quad (7)$$

Beltrami coefficient μ relates both magnitude and angle of the dilation of surface. Fig. 3 shows the relation between Beltrami coefficient μ and shape dilation. Mathematically, if an infinity small circle is transformed to an ellipse, the distortion of the translation is $K = \frac{1 + |\mu|}{1 - |\mu|}$ and the maximal dilation direction is the argument of μ.

In the discrete setting, Beltrami coefficient can be estimated on each triangular face, based on the fact elements in the metric tensor $g(x, y)$ can be defined on each triangular face. For the purpose of simplicity, we further define the Beltrami coefficient μ_i on each vertex v_i as the area weighted average of neighboring faces,

$$\mu_i = \frac{\sum_{j,k} \mu_{[v_i, v_j, v_k]} Area([v_i, v_j, v_k])}{\sum_{j,k} Area([v_i, v_j, v_k])}. \quad (8)$$

E. Descriptor Re-sampling and Patch-Based Sparse Coding

Although the Beltrami coefficient can be extracted for each vertex or face, unfortunately, there are two obstacles to prevent the shape descriptor applying directly. The number of shape descriptor is not consistent across subjects, and the dimension of the descriptor is too high leading the scenario of curse of dimensionality where the generalization of classifier is poor.

To tackle the first obstacle, we align the unit spheres via a rotation on sphere and re-sample consistently on sphere. Denote the target unit sphere as S_t. Given a unit sphere mapping result S_q, we find a rotation (θ, ϕ) applied to S_q, such that the mean curvature difference is minimal. Although this process is not globally optimal, a good initial guess, e.g. from Freesurfer [13], leads the result quite stable. Later we re-sample the aligned unit sphere with a template triangular mesh on sphere. while the template can be arbitrary, for the favor of well sampling and simplicity, some restriction should be applied. Here, we take the attractive spherical geodesic grids scheme, where each triangle on sphere is of same area and each vertex share a consistent adjacent information, to generate a template. Geodesic grids schemes have been successfully applied to many of the problems associated with fluid-flow

simulations in a spherical geometry [23]. Now, we got the template and we can re-sample the feature values of each template point.

To walk around the second obstacle, the patch-based sparse coding [24] is taken to reduce dimensions. Patch-based sparse coding has been successfully applied to cortical surface classification [25], [26].

Here, we first collect vertexes around a vertex such that these vertexes can be reached within visiting k connected edges. We call all vertexes, with certain order, as k– ring patch of the center vertex. Fig. 4(f) shows a 4– ring patch of the center (green) vertex, in a count-clock-wise order. Since we adopt spherical geodesic grids as template, the k–ring patch can share a common graph structure. Denote P_i as the patch formed by center vertex v_i, then each patch feature P_i can be expressed by a vector $\mathbf{p}_i$. We randomly take sufficient center vertexes and form a patch for vertex, denoted as $X = (p_1, p_2, \cdots, p_n) \in \mathbb{R}^{|p| \times n}$, where each patch $p_i \in \mathbb{R}^{|p|}$ is a vector with $|p|$ elements, and the total number of patches is n

For each patch $\mathbf{p}_i$, the sparse feature extraction can be incorporated with following problem,

$$\min f_i(D, z_i) = \frac{1}{2}\|D\mathbf{z}_i - \mathbf{p}_i\|_2^2 + \lambda\|\mathbf{z}_i\|_1, \quad (9)$$

where λ is the regularization parameter.

In this way, the patch vector $\mathbf{p}_i$ is represented by an m–dimensional vector $\mathbf{z}_i$, with $m \ll |p|$. Later, the max-pooling is adopted for all the patches, $F(j) = \max\{[\mathbf{p}_1(j), \mathbf{p}_2(j), \cdots, \mathbf{p}_n(j)]\}, j = 1,2, \cdots, |p|$ to reduce the dimensions. We take $F \in \mathbb{R}^{|p|}$ as the subject's feature for classification.

III. Process Pipeline

We summarize the whole the pipeline in Fig. 4. First, the MRI images are acquired from the Alzheimers Disease Neuroimaging Initiative (ADNI) project [27]. Fig. 4(a) shows several image slices of same subject.

With the given MRI images, we adopt FreeSurfer [13] to obtain the cortex pial surfaces, as shown in Fig. 4(b). Then we follow the method introduced in Alg. 1, to obtain the unique spherical area-preserving mapping, as shown in Fig. 4(c) . Later, we extract Beltrami coefficient for each vertex. After a rough registration, we re-sample the Beltrami coefficient on unit sphere. Fig. 4(e) shows the resampling points on sphere. Finally, surface patches are generated and the feature vector for classification is formed.

IV. Data Collection

Currently, most of brain imaging researchers use the clinical symptom-based diagnosis without the confirmation of beta-amyloid plaques (Aβ) in human brains. In this work, we study whole-brain morphometry on a cohort consisting of Aβ positive AD (N=151) and

matched Aβ negative cognitively unimpaired subjects $N = 271$ with Aβ positivity determined via florbetapir PET. The demographic information of subjects is given in the Table I.

V. EXPERIMENTAL RESULTS

A. Group Difference

Our area-preserving mapping preserves the global connectivity and local area of each vertex, so it reflects the local structure of cortical surface with great fidelity.

For each re-sampled point, we simply add its vertex's coordinate across all subjects. This yields the average shape as shown in Fig. 5. We see the major gyri/sulci structures are well preserved in the average brain surface. It demonstrates that our mapping is quite easy for future registration work, given the fact that a simple alignment keeps major structure in the average surface.

With the average brain surface, we can further visualize the difference of shape descriptors between two study groups. We take the average shape descriptor on each group (simply add the feature descriptor on each re-sampled vertex among the subjects in the same group). Fig. 5 color shows the feature value difference. We notice stronger shape difference in the medial temporal lobe (MTL) area. It agrees with prior AD studies [12] which have shown that the MTL is one of the most vulnerable regions and earliest affected due to AD progression.

B. Classification

We further test shape descriptor performance on classifying cortical surfaces from different clinical groups. We use 80% of the left hemisphere of the pial surfaces to train a SVM classifier and use the remaining 20% to validate. This process is repeated by 500 times, and the results of average classification rate and sensitive rate are shown in Table II. The proposed method is compared with popular brain measures, the spherical harmonic mapping [20], weighted spherical harmonic mapping [28], and the thickness as a feature patch-based sparse coding [24].

While we refer the readers to the paper [28] for details of weighted spherical harmonic mapping, we briefly introduce the idea to introduce necessary notations. A function, defined on sphere, can be represented as, $p(\theta, \phi) = \sum_{l=0}^{l=L} \sum_{m=-l}^{l} c_{lm} e^{-l(l+1)w} Y_{lm}(\theta, \phi)$. Y_{lm} is the spherical harmonic basis, w is the weight value, and c_{lm} are the coefficients. When $w = 0$, equation is degenerated to conventional spherical harmonic decomposition [20]. In the experiment of Weighted Spherical Harmonic classification, we apply the decomposition for each coordinate channel one by one, namely X, Y and Z, with $L = 100$, and optimized w [28]. Then collect coefficients $\{c_{lm}\}$ of each channel and combine all the coefficients as a vector. The same issue is that the dimension of coefficients is too high, thus we apply sparse coding scheme as discussed in Eq. 9 (regard the coefficients as a single patch) to prune the representative features. The performance SVM classifier with Weighted Spherical Harmonic as the feature is illustrated in the second row of Tab. II. The same process is repeated for $w = 0$, that is the classifier with Spherical Harmonic coefficient as the feature (first-row method

in Tab. II). Another method we compared is the thickness based surface sparse coding (third-row method in Tab. II). It shares a similar approach to our method, the differences are, the alignments comes from the result of Freesurfer, and the feature is cortical thickness instead of Beltrami coefficient.

Our method can out-perform the (weighted) Spherical Harmonic method. Compare to spherical harmonic coefficient sparse coding, our scheme takes a patch-based sparse coding scheme, it greatly empowered the method. On the other hand, we compare our method with the thickness based patch sparse coding approach. Our method still outweighs, indicating that the improvement is not only contributed by patch-based sparse coding, but also the good selection of shape descriptor.

VI. Conclusion and Future Work

In this paper, we incorporated several state of the art methods to map the cortical surface onto a unit sphere, extract shape descriptor on the unit sphere, re-sample the shape descriptor, generate patches on sphere, and classify the normal controls and AD patients with SVM. The results show that the proposed shape descriptor is sensitive for surface deformation and thus can detect AD's influence on the brain surface. We also discussed the shape descriptor for the two groups. The results explain the reason why our shape descriptor can detect the shape abnormality affected by AD.

There are some opportunities to refine our current work. For instance, during the surface reregistration, we could slightly adjust each vertex position to minimize the curvature difference.

Acknowledgments

Research is supported in part by NIH (R21AG049216, RF1AG051710, R01EB025032, U54EB020403, R01AG031581 and P30AG19610) and NSF (DMS-1413417 and IIS-1421165)

References

1. Alzheimers disease facts and figures. Alzheimers Association; 2017.
2. Sperling RA, et al. Toward defining the preclinical stages of Alzheimer's disease: recommendations from the National Institute on Aging-Alzheimer's Association workgroups on diagnostic guidelines for Alzheimer's disease. Alzheimers Dement. May; 2011 7(3):280– 292. [PubMed: 21514248]
3. Vemuri P, Jack CR. Role of structural MRI in Alzheimer's disease. Alzheimers Research & Therapy. 2010; 2(4):10.
4. Caselli RJ, Reiman EM. Characterizing the preclinical stages of Alzheimer's disease and the prospect of presymptomatic intervention. J Alzheimers Dis. 2013; 33(Suppl 1):S405–416. [PubMed: 22695623]
5. Frisoni GB, et al. The clinical use of structural MRI in alzheimer disease. Nature Reviews Neurology. 2010; 6(2):67– 77. [PubMed: 20139996]
6. Liu J, et al. Classification of Alzheimers disease using whole brain hierarchical network. TCBB. 2016:1–1.
7. Hua X, et al. Mapping Alzheimer's disease progression in 1309 MRI scans: Power estimates for different inter-scan intervals. NeuroImage. May; 2010 51(1):63–75. [PubMed: 20139010]
8. Wang Y, et al. Surface-based TBM boosts power to detect disease effects on the brain: An N = 804 ADNI study. NeuroImage. Jun; 2011 56(4):1993–2010. [PubMed: 21440071]

9. Wang G, et al. A novel cortical thickness estimation method based on volumetric LaplaceBeltrami operator and heat kernel. Medical Image Analysis. May; 2015 22(1):1–20. [PubMed: 25700360]
10. Shen D, Davatzikos C. HAMMER: hierarchical attribute matching mechanism for elastic registration. T-MI. Nov; 2002 21(11):1421–1439.
11. Christensen GE, et al. Deformable templates using large deformation kinematics. IEEE Trans Image Process. 1996; 5(10):1435–1447. [PubMed: 18290061]
12. Thompson PM, et al. Mapping cortical change in Alzheimer's disease, brain development, and schizophrenia. Neuroimage. 2004; 23(Suppl 1):2–18.
13. Fischl B, et al. Cortical surface-based analysis: Ii: Inflation, flattening, and a surface-based coordinate system: Ii: Inflation, flattening, and a surface-based coordinate system. NeuroImage. Feb; 1999 9(2):195–207. [PubMed: 9931269]
14. Shi J, et al. Conformal invariants for multiply connected surfaces: Application to landmark curve-based brain morphometry analysis. Medical Image Analysis. 2017; 35:517–529. [PubMed: 27639215]
15. Lai R, Shi Y, Scheibel K, Fears S, Woods R, Toga AW, Chan TF. Metric-induced optimal embedding for intrinsic 3d shape analysis. 2010 IEEE Computer Society Conference on Computer Vision and Pattern Recognition; June 2010; 2871–2878.
16. Chung MK. Computational neuroanatomy the methods. Teaneck, NJ: World Scientific; 2013.
17. Bronstein MM, Bronstein AM. Shape recognition with spectral distances. TPAMI. May; 2011 33(5):1065–1071.
18. Sun J, et al. A concise and provably informative multiscale signature based on heat diffusion. Computer Graphics Forum. Jul; 2009 28(5):1383–1392.
19. Su Z, et al. Optimal mass transport for shape matching and comparison. TPAMI. Nov; 2015 37(11):2246–2259.
20. Gu X, et al. Genus zero surface conformal mapping and its application to brain surface mapping. T-MI. Aug; 2004 23(8):949– 958.
21. Xianfeng Gu FL, et al. Variational principles for Minkowski type problems, discrete optimal transport, and discrete MongeAmpre equations. Asian Journal of Mathematics. 2016; 20(2)
22. Gardiner FP. Quasiconformal Teichmller theory. Providence, R.I: American Mathematical Society; 2000. ser. Mathematical surveys and monographs ; no. 76
23. Williamson DL, et al. A standard test set for numerical approximations to the shallow water equations in spherical geometry. Journal of Computational Physics. 1992; 101(1):227–228.
24. Zhang J, et al. Empowering cortical thickness measures in clinical diagnosis of alzheimer's disease with spherical sparse coding. Proceedings IEEE ISBI. Apr.2017 2017
25. Zhang J, , et al. Multi-source multi-target dictionary learning for prediction of cognitive decline. International Conference on Information Processing in Medical Imaging; Springer; 2017. 184–197.
26. Zhang J, , et al. Hyperbolic space sparse coding with its application on prediction of alzheimers disease in mild cognitive impairment. International Conference on Medical Image Computing and Computer- Assisted Intervention; Springer; 2016. 326–334.
27. ADNI. http://adni.loni.ucla.edu
28. Chung MK, et al. Weighted fourier series representation and its application to quantifying the amount of gray matter. IEEE transactions on medical imaging. Apr.2007 26(4)

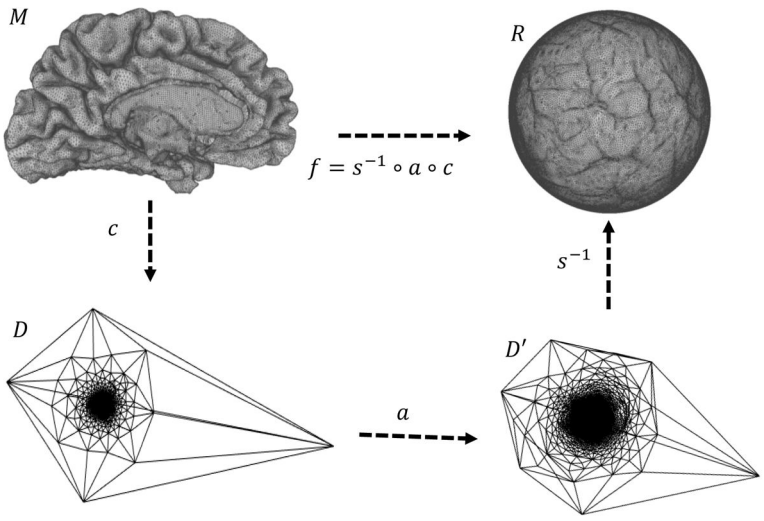

Fig. 1.
Global optimal area-preserving mapping.

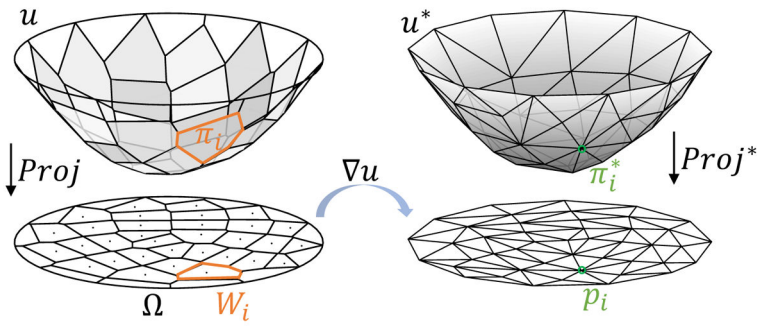

Fig. 2.
Discrete transport plan of ∇u.

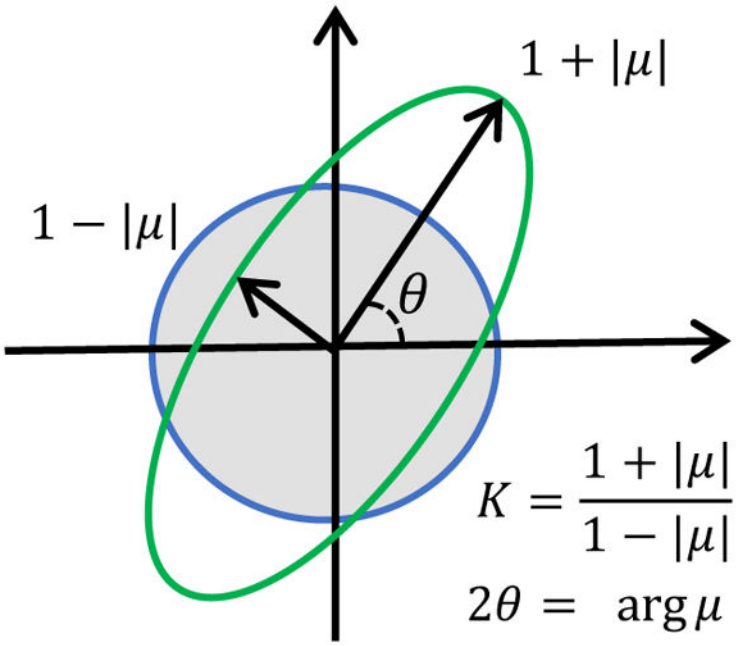

Fig. 3.
Beltrami coefficient measures the map dilation.

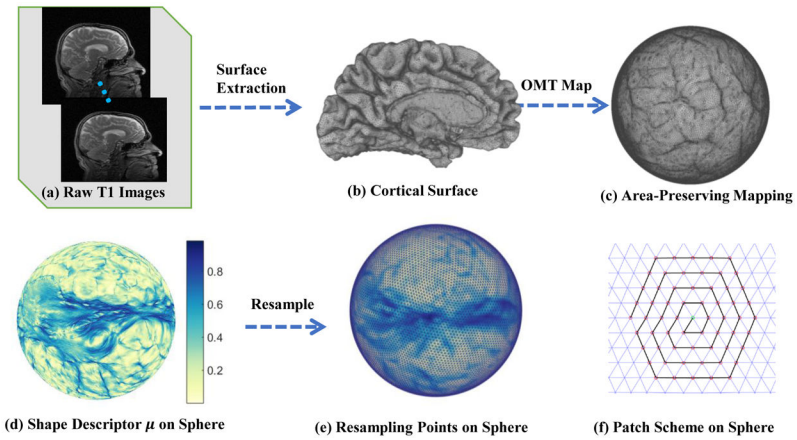

Fig. 4.

Process Pipeline: (a) is the MRI images; (b) is the extracted cortical surface; (c) is the area-preserving mapping result; (d) shape descriptor on sphere; (e) consistent shape descriptor on sphere; (f) patch of green vertex

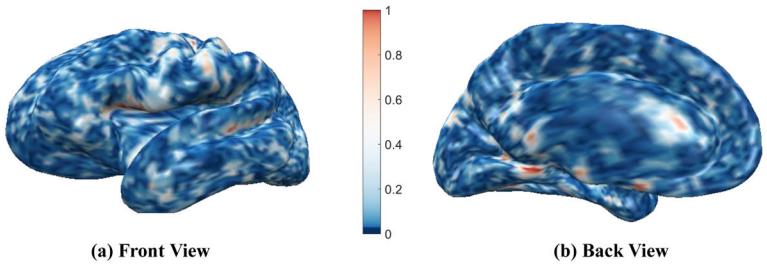

Fig. 5.
Shape descriptor difference overlaid on the average brain surface.

TABLE I

Demographic information of subjects in this study

Group	Size	Gender M/F	Age	MMSE
AD (Aβ+)	151	79/72	74.5± 7.9	22.6± 3.1
NL CTL (Aβ−)	271	132/139	76.3± 6.7	29.0± 1.3

TABLE II

Average recognition rate of different signatures

Method	Accurate(%)	Sensitivity(%)
Spherical Harmonic	77.5	65
Weighted Spherical Harmonic	80.0	77.78
Thickness Sparse Coding	77.9	66.67
Proposed Shape Descriptor	**81.8**	**80.8**